

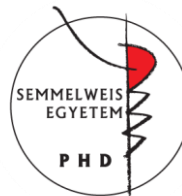
Dendritic Ca²⁺ Spikes and Interneuronal Ripple Oscillations in Fast Spiking Parvalbumin Containing Interneurons during Hippocampal Sharp Wave-Ripple activities

Doctoral Thesis

Balázs Chiovini

Semmelweis University

János Szentágothai Doctoral School of Neurosciences



Supervisor: Balázs J. Rózsa PhD

Official referees: Zita Puskár PhD
Árpád Mike PhD

Chairman of the
final examination board László Tretter DSc

Members of the
final examination board: István Ulbert PhD
Árpád Dobolyi PhD

Budapest
2015

1. Introduction

Hippocampal fast-spiking, parvalbumin-expressing interneurons (FS-PV INs) play important roles in synchronized oscillations and information processing during sharp wave-ripple activities (SPW-Rs). Several facts suggest that SPW-R-associated cell assemblies can activate dendritic hot-spots, but the relationship between SPWs, field ripple oscillations and dendritic hot-spots have not yet been studied. Until now it was not possible to examine the dendritic signal processing in the long and thin dendrites of FSPV-INs during SPW-R oscillations. The question how these neurons can organize such a large inputs arriving during SPW-Rs to the extended dendritic arbour and form output of the cells remains elusive. To answer these questions, I introduce a new type of experiments where almost the whole dendritic arbour can be measured simultaneously in 3 dimension (3D) in real time with a novel 3D random access two-photon microscope.

1.1. Hippocampal circuits

The hippocampus has two main loops. The long or so-called trisynaptic loop follows the layer 2 entorhinal cortex (EC), granule cells of the dentate gyrus, CA3, CA1 and subiculum containing axis of the hippocampus with multiple short cuts and superimposed loops. The short excitatory loop is formed between the EC layer III and CA1 directly which is then projected back to the EC layer V. Along these loops the main hippocampal oscillations are formed, namely the theta (4-12 Hz), the gamma (30-80 Hz) and the SPW (0.5-1.5Hz) with superimposed ripple (140-200 Hz) activities. Depending on the behavioural state of the animal, these oscillations form a well defined flow direction on the cortico-hippocampal axis. During consummatory behaviour and slow-wave sleep SPW-R activities appear. These hippocampal patterns are responsible for the encoding, storage and retrieval of memory. This sensitive dialogue forms the short term memory into long term memory transition with specific steps.

1.2. Properties of SPW-R complexes

SPW activity is a unique self organized endogenous rhythm of the hippocampus. It is characterized by a high amplitude and relatively slow oscillation (0.5-1.5Hz). A SPW event can propagate along the hippocampal CA regions from CA3 to CA1 and activates locally the different pyramidal cell - inhibitory cell assemblies. The CA3 and CA1 SPWs are associated by fast gamma (90-140Hz) or ripple activities at 140-200Hz frequencies which are activated locally, led by the SPWs and synchronized by the local interneuronal sub-networks. The initiation of the SPW-R complexes is driven by an interaction between hippocampal excitatory pyramidal cells and inhibitory neurons, especially local perisomatic region-targeting interneurons. Recent studies indicate the ripple timing can be set by the interaction between PV INs. The strong tonic excitatory drive evokes high frequency firing in PV basket cells and their reciprocal inhibitory activity is essential for coherence. The potential role of the synchronized CA1 ripples is to amplify the output messages of the hippocampus. They synchronize and coordinate local pyramidal cell activity, select the dominant and suppress the competing neuronal assemblies and propel forward to the cortical and subcortical structures.

1.3. Features of FS-PV INs

FS-PV INs are a subclass of interneurons which could be well-identified by distinct electrophysiological properties and molecular markers. In the stratum pyramidale of CA1 three types of PV-containing interneurons exist: PV basket cells, axo-axonic cells and bistratified cells. According to Pettilla terminology, they are all fast spiking interneurons. These interneurons selectively express the Ca^{2+} binding protein, called parvalbumin (PV) which can be found in every compartment of the cell. The extended thin, aspiny dendritic and axonal arbour, the number of synapses and boutons, the ion channel distribution and types help to facilitate the generation of fast excitatory postsynaptic potentials (EPSPs) on PV INs. These features of FS-PV INs assist the better and faster information flow from the input of the

cell to its output, to axonal boutons, which are equipped with machinery for fast transmitter release.

1.4. Dendritic integration and role in SPW-R oscillation of fast spiking PV interneuron

Several facts suggest that SPW-R-associated cell assemblies can activate dendritic hot-spots, but the relationship between SPWs, field ripple oscillations and dendritic hot-spots have not yet been studied. However, how and why these SPW-R-associated cell assemblies activate dendritic hot-spots and if this activation changes the dendritic computation and AP output of individual neurons, have not been investigated yet. According to the generally accepted view, FS-PV INs act in cortical circuits as fast and, essentially, passive integrators of synaptic inputs. Several papers support the passive properties of FS-PV INs: accelerated kinetics of excitatory postsynaptic potentials (EPSPs), a reduced, sub-millisecond temporal window for dendritic integration, and precise and fast coupling between EPSPs and AP outputs. Ca^{2+} dynamics have been found to be fast in the aspiny dendrites of FS-PV INs and are strongly related to approximately 1 μm long, dendritic microdomains. According to the literature, regenerative dendritic spikes cannot be evoked in these cells and back-propagating APs are severely attenuated. However, dendritic integration and EPSP-AP coupling can be different under high-activity conditions such as SPW-Rs when neurons receive precisely timed dendritic inputs

2. Aims

- I. One of my main goals was to reveal active, regenerative Ca^{2+} events (spikes) in dendrites of FS-PV INs during spontaneous SPW-R activities.
- II. Secondly, I addressed the connection between dendritic spontaneous Ca^{2+} events and the associated membrane potential signals to examine the input-output transformation of the cells.
- III. My third aim was to define how many inputs are required to evoke regenerative Ca^{2+} events in the distal dendrites of FS-PV INs and to specify the nonlinear dendritic integration mechanisms in the generation of Ca^{2+} events and the associated membrane potential signals in FS-PV INs.
- IV. Finally, I clarified the types of ion channels, which play a role in the generation and propagation of dendritic Ca^{2+} events and membrane potential signals.

3. Methods

3.1. Mouse line and electrophysiology

Horizontal acute brain slices were prepared from transgenic mice expressing enhanced green fluorescent protein (eGFP) controlled by the parvalbumin promoter. Whole-cell recording was performed from FS-PV INs in the CA1 region. In the dual ‘superfusion’ chamber both surfaces of the 450 μm -thick slice were perfused with >10 ml/min. LFP (from str. pyr. of the hippocampal CA1 region) and juxtacellular signals were recorded using glass electrodes (6-9 M Ω) filled with artificial cerebrospinal fluid.

3.2. Pharmacology

All drugs were applied in the bath, except during local TTX injection (10 μM). Tetrodotoxin (TTX) (1 μM), nimodipine (20 μM), mibefradil (10 μM), ω -conotoxin MVIIC (0.5 μM), 6-cyano-2,3-dihydroxy-7-nitro-quinoxaline (CNQX) (10 μM), and D,L-2-amino-5-phosphonopentanoic acid (DL-AP5) (60 μM) were purchased from Tocris Bioscience. The cocktail of voltage-gated calcium channel (VGCC) blockers contained ω -conotoxin MVIIC, nimodipine, and mibefradil as well.

3.3. Two-photon imaging

Analysis was performed with MATLAB-based program (MES, Femtonics) using custom-written software elements. In this study, we improved our 3D-AO imaging and trajectory scanning method. Spatial resolution and scanning volume was also increased by about 20% and 10%, respectively, by optimizing the system for the new XLUMPlanFI20 \times /1.0 objective lens (Olympus, 20 \times , NA 1.0). New software modules were developed for fast 3D dendritic measurements and to compensate for sample drift. The 3D raw green fluorescent data

(F) were collected along the dendrite, spatially normalized, and then projected onto a two-dimensional plot (defined as 3D Ca^{2+} responses) by applying the formula: $\Delta F/F = (F(d,t) - F_0(d))/F_0(d)$ or $\Delta G/R = (F(d,t) - R(d))/R(d)$.

3.4. Two-photon uncaging experiments

To simulate dendritic Ca^{2+} spikes DNI-Glu•TFA (2.5 mM) was used which was applied in the bath. The uncaging wavelength was set to 740 nm according to the red-shifted two-photon optimum. In simultaneous two-photon uncaging and imaging measurements the Roller Coaster Scanning method was used.

3.5. Data analysis and statistics

All neuronal input-output curves could generally be characterized by an initially concave or linear curve ($y_1 = A_1(1 - e^{(-A_2*(x-A_3)})$), on top of which a sigmoid-like supralinear increase was superimposed at a given threshold input number ($y_2 = \frac{A_4}{1 + e^{\frac{(x-A_5)}{A_6}}} + A_7$).

Threshold input numbers were generally defined as the smallest active input numbers above the sigmoidal increase. Relative fluorescence changes were transformed to Ca^{2+} concentration change using the

$$\frac{\Delta Ca}{K_D} = \frac{f_{\max}}{f} (1 - R^{-1}_f) \frac{\delta f}{(\delta f_{\max} - \delta f) \delta f_{\max}}. \quad \text{The statistical}$$

difference was measured using the Student t-test (*, **, or *** indicate p values of less than 0.05, 0.01, or 0.001, respectively). If not otherwise indicated, data are presented as means \pm s.e.m.

3.6. Detection of interneuronal ripple oscillations using the baseline subtraction method

Band-pass filtering can generate extra oscillation events and phase shifts when the filtered oscillations are irregular, which is the case for SPW-associated ripple oscillations. To avoid these errors, in the first step we used Gauss filtering (100 Hz) on the raw traces to generate a “baseline”, which was then subtracted from the raw traces to better preserve the amplitude and phase of the individual ripple oscillation cycles.

4. Results

4.1. Recording of spontaneous SPW-R activity *in vitro* using a modified dual superfusion recording chamber and fast perfusion rate

For the better oxygenation of slices, I used a modified dual superfusion-type chamber; where the perfusate was flow (11.2ml/min) below and above the slices. The samples were placed on a mesh. Under such conditions the slices could generate neuronal network oscillations. On the other hand, the dual superfusion chamber was modified for better imaging as well. The slice supporting metal mesh was exchanged to a nylon mesh and it was lowered to match the working distance of a high numeric aperture (NA) condenser. The optical aperture of the chamber was increased to be optimized for multi-channel recordings and for the application of high NA objectives with small working distances. In the dual superfusion chamber, SPW-R activities could be recorded because of the better oxygenation. Under our recording conditions, SPW events occurred spontaneously at a rate of 1.44 ± 0.09 Hz ($n=32$) and were associated with network ripple oscillations (f_{\max} 249.2 ± 12.7 Hz) using $450 \mu\text{m}$ thick slices. Therefore, according to the previous observations, the dual superfusion chamber with an increased flow rate provides better recording conditions, which can maintain physiological network oscillations such as SPW-Rs.

4.2. SPW-R-associated dendritic input patterns

Simultaneous trajectory scanning in 3D was performed along the multiple dendritic segments (up to $700 \mu\text{m}$ in length) during SPW-R activities. According to the previous published data and support the passive nature of FS-PV INs somatically evoked bAP Ca^{2+} in FS-PV IN dendrites show non uniform manner, and decreased below the recording threshold at a short distance from the soma ($113.88 \pm 14.50 \mu\text{m}$, $n=13$). In contrast to this the spontaneous SPW-R related AP (SPW-APs) and SPW-R related EPSPs (SPW-EPSPs) Ca^{2+} signals

show increased manner as a function of a distance from the soma. Furthermore the somatically recorded subthreshold events related SPW-R (SPW-EPSPs) show similar feature. In our *in vitro* preparations, SPW-EPSP-associated network activities which induced locally clustered responses, termed dendritic hot-spots (FWHM: $3.73 \pm 0.13 \mu\text{m}$), which was also able to generate more generalized signals, which invaded continuous dendritic segments of the distal apical, but not the basal dendritic arbor. These data support the idea that the passive FS-PV INs can switch from a ground state to an excited, active state when the neuronal networks are active generating a changed dendritic integration status. Thus at the excited state, regenerative dendritic activities, such as propagating dendritic Ca^{2+} spikes, could occur.

4.3. Dendritic spikes are associated with interneuronal ripple oscillations

The Ca^{2+} signal amplitude in average was well-correlated with the amplitude of the subthreshold somatic activity induced by SPW-EPSPs and with the numbers of the SPW-APs. I noticed that the Ca^{2+} signal amplitude accompanied specifically with larger SPW-EPSPs with long oscillating plateau-potentials than SPW-APs. The oscillation frequencies were at ripple range, therefore these oscillations were named as *interneuronal ripple activities*. The oscillation frequency was rapidly increased before the SPW-EPSP peak, it reached the maxima at the peak ($f_{\text{max}} 270.3 \pm 18.18 \text{ Hz}$, $n=11$) and slowly decreased after the peak ($239.97 \pm 19.25 \text{ Hz}$), while its duration extended $17.1 \pm 3.19 \text{ ms}$ beyond the termination of the network LFP signal (LFP FWHM $12.23 \pm 1.85 \text{ ms}$, EPSP FWHM $29.37 \pm 2.49 \text{ ms}$, $p=0.0001$). The membrane potential oscillations on the plateau were more elongated than the simultaneously recorded LFP oscillations; they indicate the intrinsic oscillatory properties of the FS-PV INs. The amplitude of SPW-EPSP associated Ca^{2+} responses were well-correlated with the power of the interneuronal ripple oscillations in spatial averages across dendrites and in individual dendritic segments. The interneuronal ripple activities showed similar frequency and phase values in both

cases, SPW-EPSPs and SPW-APs (239.97 ± 18.35 Hz and 239.70 ± 11.00 Hz, respectively, $p > 0.3$, $n = 10$). The output of the cells were precisely phase locked to the peak of the interneuronal ripple activities, indicating that the dendritic spikes induced by synchronized network activities could transiently switch the input-output transformation function of FS-PV INs from the well-characterized sub-millisecond precision of EPSP-AP coupling to a slower integration scale, where interneuron output is gated in phase synchrony with interneuronal ripple oscillations.

4.4. Characterizes of the SPW-R associated dendritic Ca^{2+} spikes

Large 3D Ca^{2+} responses were detected during both SPW-EPSPs and SPW-APs as well. This Ca^{2+} invades the whole apical dendritic region with non uniform manner. There were several local maxima along the apical arbor where the Ca^{2+} signal amplitudes were significantly higher, called hot-spots. In these hot-spots the Ca^{2+} responses were not only larger than the Ca^{2+} responses record in the neighboring dendritic segment ($333\% \pm 51\%$, $n = 17$ regions in $n = 9$ cells), but emerge earlier at 12.8 ± 2.4 ms (41.5 ± 12.7 μm from the center of the hot-spot), indicating that the hot-spots are the initiation site of the dendritic calcium spikes. The Ca^{2+} spike invade both centripetally and centrifugally from the hot-spots. Supporting the regenerative nature of the dendritic spikes, the propagation speed from the hot-spots toward lateral dendritic segments could be clearly measured in 68.8 ± 8.2 % of long dendritic segments (222.1 ± 63.0 μm , $n = 13$), yielding an average propagation speed of 34.22 ± 4.32 $\mu\text{m}/\text{ms}$, a substantially higher speed than that expected from diffusion. These Ca^{2+} spikes which associated the SPW-EPSPs never propagated from the soma, suggesting their dendritic origin. These signals showed regenerative nature and actively propagated from dendritic hot-spots.

4.5. Spatially and temporally clustered inputs generate the dendritic spikes

Ca²⁺ responses were evoked point by point by glutamate uncaging in a well-localized region of the dendrite. SPW-R associated hot-spots in this way could be reproduced by glutamate uncaging. I found that the uncaging evoked Ca²⁺ responses in the hot-spot-like regions showed a step-like nonlinear increase at a well defined active input number, identified the first threshold (11.04±1.4 active inputs, n=9 cells). The first threshold was followed by a second one which was clearly visible outside the input zone (hot-spot-like zone) termed lateral dendritic region where the evoked Ca²⁺ responses show a sigmoid-like increase. The active input number at the second threshold was 30.3±4.0 (range 10-47 n=9 cells). As the average release probability of excitatory synapses onto FS-PV INs is 0.75±0.19, the first and second threshold of active input numbers correspond to the activation of around 15 and 40 release sites, respectively.

4.6. Characterizes of the uncaging evoked dendritic Ca²⁺ spikes

The uncaging evoked dendritic Ca²⁺ therefore could be separated to two parts a hot-spot like input region where activated synapses were localized and a lateral dendritic region. The spatial distribution of the Ca²⁺ increase in the lateral dendritic regions showed a plateau-like characteristic above the second threshold. The amplitude of the Ca²⁺ plateau was slightly decreased as a function of a distance from the input region. The propagation speed could also be estimated resulting in 17.4±3.6 μm/ms in 85.1±16.4 μm-long dendritic segments (n=5 cells), which speed is similar to the propagation speed of the large, spontaneous SPW-EPSP-associated dendritic 3D Ca²⁺ responses.

4.7. Activation of a short dendritic segment by glutamate uncaging can generate interneuronal ripple oscillation

Until the second threshold the amplitude of the uncaging evoked EPSPs were showed similar step-like increasing manner - like the Ca^{2+} response. This initial linear or sublinear increase progressively jumped at the second threshold and shows supralinear characteristic as a function of an increasing number of active inputs. However, at 40 inputs on the FS-PV INs, the responses reached the second threshold (2nd thr.) and a sigmoid-like increase in EPSP amplitudes was superimposed on the sublinear input-output curve. Somatically recorded interneuronal ripple oscillations could be detected above the second threshold. The frequency of spontaneous SPW-EPSPs associated interneuronal ripple activities was 239.97 ± 18.35 Hz. The frequency of uncaging evoked interneuronal ripple oscillation was 219.3 ± 14.5 Hz similar to that found for the spontaneous one. Dendritic Ca^{2+} responses were 41.8 ± 9.6 % larger when interneuronal ripple activities could appear on the top of the evoked EPSPs ($p=0.008$; $n=6$ cells). The frequency of the evoked interneuronal ripple oscillations were similar ($p=0.23$, t -test, $n=7$), but distributed input patterns induced ripple range oscillations in more dendritic segments (73.68%, 14/19 segments in 14/19 cells) and produced more oscillation cycles upon each induction. APs were strongly coupled to the peaks of the ripple oscillations. These data imply that the well-known fast, reliable EPSP-AP coupling of FS-PV INs is replaced during periods of strong excitation by a new integration mode where the timing of AP output is determined primarily by the phase of interneuronal ripple oscillations.

4.8. Ca^{2+} spikes are mediated by L-type VGCCs

Dendritic Ca^{2+} signals are dominantly triggered by AMPA (2-amino-3-(5-metil-3-oxo-1,2-oxazol-4-il) and NMDA (N-methyl-D-aspartate) receptors, thus as we expected the combined application of AMPA and NMDA receptor blockers (CNQX and AP5, respectively) reduced the Ca^{2+} signals almost to zero in both, hot-spot and lateral regions. In the lateral dendritic region the cocktail of VGCC blocker

evoked great reduction in Ca^{2+} signal. We found that the most important VGCC is the L-type one, because when we applied its specific blocker the Ca^{2+} signal reduced the most. In the central, hot-spot region the dependency of the VGCC on the Ca^{2+} signal is more complex, because it is mediated in parallel by NMDA, calcium permeable AMPA receptors and VGCC, moreover further amplified by Na^+ channel. In line with other observations, I noted that Ca^{2+} -permeable AMPA receptors had a larger effect on the postsynaptic Ca^{2+} influx than NMDA receptors.

4.9. Interneuronal ripple oscillation are mediated by dendritic Na^+ channels

The Na^+ channel blocker totally abolished the interneuronal ripple oscillations, indicating the crucial role of these channels to create this phenomenon. Application of AP5, nimodipine, IEM-1460 or the cocktail of VGCC blockers did not change significantly the frequency of the oscillations. In order to validate more the dendritic origin of interneuronal ripple oscillations, TTX (10 μM) was injected onto the axosomatic region of the FS-PV INs, while clustered glutamate uncaging was evoked on the distal dendritic area as previously described. The frequency of the interneuronal ripple activities which was evoked by spatiotemporally clustered glutamate uncaging did not change significantly (control 212.83 ± 24.18 Hz; TTX puff 182.72 ± 18.72 Hz, paired t-test, $p=0.156$), indicating that the oscillations had indeed dendritic origin. To detect dendritic local membrane potential oscillations more directly, whole cell patch clamp and dendritic juxtacellular recordings (266.37 ± 67.05 μm , mean \pm s.d. from the soma at the uncaging site) were combined. The juxtacellular recording interneuron ripple oscillation amplitude was totally diminished in 40 μm (spatial decay constant 15.6 ± 4.9 μm , $n=4$) from the uncaging evoked dendritic area. These data strongly support the dendritic origin of the interneuronal ripple oscillations. In summary, I can conclude that dendritic spikes exist in FS-PV INs.

5. Summary and conclusion

Hippocampal FS-PV INs and their crucial role in the generation of SPW-Rs are intensively studied mainly in electrophysiological measurements. Moreover, with confocal and two-photon imaging techniques the mechanism of dendritic integration in FS-PV INs' dendrites is also an important and studied area of neuroscience. But the relationship between the two important topics couldn't have been examined. To achieve this, recently developed 3D and 2D two-photon imaging techniques and new glutamate uncaging material were used. In my thesis I challenge the classical view of FS-PV INs dendritic integration mode and function during the presence of spontaneous SPW-Rs.

First, AP-associated Ca^{2+} responses are not compartmentalized to the proximal dendritic regions but also invade distal dendritic segments during SPW-Rs. Dendritic spikes occur, in contrast to the low-activity baseline state.

Second, I found that supralinear dendritic integration with a dual-integration threshold replaces linear or sublinear summation. Compartmentalized synaptic Ca^{2+} signals are replaced by broadly propagating Ca^{2+} waves which are generated at dendritic hot-spots. Dendritic voltage-gated Na^+ channels, which are functionally inactive in low activity conditions, start to generate interneuronal ripple oscillations, which are associated with the dendritic Ca^{2+} spikes.

Third, I found that the integration mode of FS-PV INs changes, AP outputs are tightly coupled to the phase of interneuronal ripple oscillations, and the total time-window of AP outputs becomes broader compared to the submillisecond precision in EPSP-AP coupling that characterizes the low activity state.

Fourth, my findings indicate that propagating Ca^{2+} spikes are mainly dependent on L-type VGCC, while interneuronal ripple activities are related to non-perisomatic Na^+ channels.

I demonstrate a novel ingredient in the generation of population ripple oscillations. Synchronized inputs arrive to the CA1 FS-PV INs from CA3 and local CA1 cell assemblies which generate hot-spots and associated intrinsic ripple oscillations in distal apical dendrites of FS-

PV INs. The membrane ripple oscillations start to form few millisencond-long time windows for signal integration, than AP output is generated after some oscillation period. Our working hypothesis supports the idea that the AP output is synchronized to these interneuronal ripple oscillations, i.e. EPSPs which are in phase synchrony with the oscillations, which will amplify and contribute to the APs.

These findings support the idea that FS-PV INs during SPW-R activities switch to an excited state where regenerative, active dendritic properties can exist. These intrinsic properties of the cells have an effect on the SPW-R generation at a level of a dendritic segment. These data challenge the classical view of the dendritic and cellular properties of FS-PV INs.

6. List of the Author's Publication

6.1. Publications related to thesis

Chiovini B*, Turi GF*, Katona G, Kaszás A, Pálfi D, Maák P, Szalay G, Szabó MF, Szabó G, Szadai Z, Káli S, Rózsa B. Dendritic spikes induce ripples in PV interneurons during hippocampal sharp waves. *Neuron*. 2014 May 21;82(4):908-24. doi: 10.1016/j.neuron.2014.04.004. PMID: 24853946

** These authors contributed equally to this work.*

Chiovini B, Turi GF, Katona G, Kaszás A, Erdélyi F, Szabó G, Monyer H, Csákányi A, Vizi ES, Rózsa B. Enhanced dendritic AP backpropagation in PV-positive basket cells during sharp wave activity. *Neurochem Res*. 2010 Dec;35(12):2086-95. doi: 10.1007/s11064-010-0290-4. Epub 2010 Nov 3. PMID: 21046239

6.2. Publications independent from thesis

Katona G*, Szalay G*, Maák P*, Kaszás A*, Veress M, Hillier D, Chiovini B, Vizi ES, Roska B, Rózsa B. Fast two-photon in vivo imaging with three-dimensional random-access scanning in large tissue volumes. *Nat Methods*. 2012 Jan 8;9(2):201-8. doi: 10.1038/nmeth.1851. PMID: 22231641

** These authors contributed equally to this work.*

Kerekes PB, Tóth K, Kaszás A, Chiovini B, Szadai Z, Szalay G, Pálfi D, Bagó A, Spitzer K, Rózsa B, Ulbert I, Wittner L. Combined two-photon imaging, electrophysiological, and anatomical investigation of the human neocortex in vitro *Neurophoton*. 1(1), 011013 (Sep 11, 2014). doi:10.1117/1.NPh.1.1.011013

6.3. Patents independent from thesis

Csizmadia IGy, Mucsi Z, Szalay G, Kaszás a, Lukácsné Haveland Cs, Majercsik O, Potor A, Katona G, Rózsa B, Gündisch D, Chiovini B, Pálfi D. Use of Photocleavable compounds. WO2012HU00100 20121003

Csizmadia IGy, Rozsa JB, Mucsi Z, Lukácsné Haveland Cs, Katona G, Majercsik O, Potor A, Kaszas A, Guendisch D, Chiovini B, Szalay G, Palfi D. Use of Photochemically cleavable compounds HU20120000574 20121003

Rózsa B, Katona G, Veress M, Maak P, Szalay G, Kaszas A, Chiovini B, Matyas P. Method for scanning along a continuous scanning trajectory with a scanner system WO2012HU00001 20120105